Molecular Biology of the Cell
Vol. 21, 131–139, January 1, 2010

Novel Role of ATPase Subunit C Targeting Peptides Beyond Mitochondrial Protein Import

Cristofol Vives-Bauza,*† Jordi Magrané,* Antoni L. Andreu,† and Giovanni Manfredi*

*Department of Neurology and Neuroscience, Weill Cornell Medical College, New York, NY 10065; and †Departament de Patologia Mitocondrial i Neuromuscular, Institut de Recerca Vall d'Hebron, 08035 Barcelona, Spain

Submitted June 15, 2009; Revised October 13, 2009; Accepted October 27, 2009
Monitoring Editor: Thomas D. Fox

In mammals, subunit c of the F_1F_0-ATP synthase has three isoforms (P1, P2, and P3). These isoforms differ by their cleavable mitochondrial targeting peptides, whereas the mature peptides are identical. To investigate this apparent genetic redundancy, we knocked down each of the three subunit c isoform by RNA interference in HeLa cells. Silencing any of the subunit c isoforms individually resulted in an ATP synthesis defect, indicating that these isoforms are not functionally redundant. We found that subunit c knockdown impaired the structure and function of the mitochondrial respiratory chain. In particular, P2 silencing caused defective cytochrome oxidase assembly and function. Because the expression of exogenous P1 or P2 was able to rescue the respective silencing phenotypes, but the two isoforms were unable to cross-complement, we hypothesized that their functional specificity resided in their targeting peptides. In fact, the expression of P1 and P2 targeting peptides fused to GFP variants rescued the ATP synthesis and respiratory chain defects in the silenced cells. Our results demonstrate that the subunit c isoforms are nonredundant, because they differ functionally by their targeting peptides, which, in addition to mediating mitochondrial protein import, play a yet undiscovered role in respiratory chain maintenance.

INTRODUCTION

F_1F_0-ATP synthase is a ubiquitous membrane protein complex that efficiently converts the transmembrane proton gradient into chemical energy stored as ATP. The enzyme is made of two molecular motors, F_0 and F_1, which are coupled by a central stalk. The membrane-embedded F_0 unit converts the proton-motive force into mechanical rotation of the central stalk inside the solvent-exposed F_1 unit. The rotation causes cyclic conformational changes in F_1, thereby driving ATP synthesis (Boyer, 2000). In mammals, the F_0 portion is made by at least 10 different subunits: a, b, c_{10}, d, e, f, g, F_6, A6L, and OSCP (Wittig and Schagger, 2008).

Subunit c (also known as subunit 9, F_0c, or lipid-binding protein) is assembled in a cylindrical c_{10} oligomer (Dickson *et al*., 2006; Walker and Dickson, 2006). Subunit c structure and function have been amply studied to clarify the mechanism coupling the proton gradient generated by the respiratory chain and ATP synthesis (Altendorf *et al*., 2000; Bulygin *et al*., 2004). Subunit c directly cooperates with subunit a (Atp6-equivalent) in the proton pumping process (Wittig and Schagger, 2008).

In yeast, subunit c (named subunit 9) is encoded by the mitochondrial DNA, whereas in plants and animals its gene has been transferred to the nucleus. In mammals, subunit c is encoded by three different genes (ATP5G1, ATP5G2, and ATP5G3), which are located on chromosomes 17, 12, and 2, respectively, and translateas into three different protein isoforms (P1, P2, and P3) (Dyer *et al*., 1989; Dyer and Walker, 1993; Yan *et al*., 1994). Mammalian subunit c consists of a mature protein of 76 amino acids, which is identical for all three isoforms, and a variable N-terminal mitochondrial targeting peptide, which is cleaved by matrix peptidases upon import. P1 isoform targeting peptide is 61 amino acids (AA), whereas P2 targeting peptide has two alternatively spliced forms of 82 AA (variant a) and 123 AA (variant b) (Dyer *et al*., 1989; Dyer and Walker, 1993; Yan *et al*., 1994). P3 targeting peptide is 67 AA long (Yan *et al*., 1994). All three subunit c isoforms are functional and contribute to the F_0 structure (Sangawa *et al*., 1997), but they have variable expression patterns in different tissues. Overall, P1 expression levels are lower than that of P2 or P3 (De Grassi *et al*., 2006).

The presence of subunit c paralogues in the proximity of HOX gene clusters in vertebrates indicates that these isoforms arose from the same segment/genome duplication event involving HOX clusters, probably during the early origins of vertebrates (Saccone *et al*., 2006). Phylogenic analyses of subunit c suggest that the three isoforms were already present before the bird–mammal divergence, but only P3 has an evident homologous gene in all analyzed vertebrates, whereas P1 is the most evolutionary divergent (Saccone *et al*., 2006).

This article was published online ahead of print in *MBC in Press* (http://www.molbiolcell.org/cgi/doi/10.1091/mbc.E09–06–0483) on November 4, 2009.

Address correspondence to: Giovanni Manfredi (gim2004@med.cornell.edu).

Abbreviations used: AA, amino acid; ATPase, F_1F_0-ATP synthase; CFP, cyanide fluorescent protein; COX, cytochrome *c* oxidase; qRT-PCR, quantitative real-time polymerase chain reaction; TMPD, *N*,*N*,*N*′,*N*′-tetramethyl-*p*-phenylendiamine; TMRM, tetramethyl rhodamine methyl ester; $\Delta\Psi_m$, mitochondrial membrane potential; YFP, yellow fluorescent protein.

Here, we have investigated the functional reasons behind the apparent genetic redundancy of the subunit c isoforms by using extensive knockdown and gene replacement approaches in human cells.

MATERIALS AND METHODS

Cell Culture and Expression Vectors

HeLa cells were cultured in DMEM supplemented with 10% fetal bovine serum, 100 U/ml penicillin, and 100 μg/ml streptomycin (Invitrogen, Carlsbad, CA).

Mouse and human P1-subunit c and P2-subunit c cDNAs were obtained from American Type Culture Collection (Manassas, VA) and subcloned into pcDNA 3.1 (Invitrogen). Hemagglutinin (HA) and myc tags were added by polymerase chain reaction (PCR) to their 3′ end, after removing the subunit c gene stop codon. P1 and P2-subunit c targeting sequences were cloned in frame into the 5′ end of both enhanced cyan fluorescent protein (ECFP) and enhanced yellow fluorescent protein (EYFP). PBOS-P1-A6-FLAG was generated previously in our laboratory (Manfredi *et al.*, 2002). All constructs were verified by sequencing.

DNA transfections were performed using FuGENE 6 (Roche Diagnostics, Indianapolis, IN) as recommended by the manufacturer. Stable HeLa cell lines expressing these constructs were generated by selection in medium containing 1 μg/μl G418 (Invitrogen).

Silencing by Small Interfering RNA (siRNA) Treatment

Specific siRNA oligonucleotides purchased from GeneGlobe (QIAGEN, Valencia, CA) were used to silence subunit c isoforms P1 (Hs_ATP5G1_5 HP Validated siRNA), P2 (Hs_ATP5G2_2 HP siRNA, Hs_ATP5G2_3 HP siRNA), and P3 (Hs_ATP5G3_5 HP siRNA). A nontargeting scrambled siRNA also purchased from QIAGEN was used as a negative control. HeLa cells (2.5×10^5) were seeded per well onto six-well plates and incubated overnight before transfection with 20 nM siRNA by using HyperFect transfection reagent (QIAGEN), according to the instructions of the manufacturer. Cells were then cultured in normal growth media for 48 h until functional assays were performed. Efficiency of gene silencing and all functional experiments were tested 48 h after silencing.

RNA Extraction and Quantitative Real-Time (qRT)-PCR

Total RNA was extracted using RNAqueous kit (Ambion, Foster City, CA) and treated with RNase-free DNase I (QIAGEN), according to the instructions of the manufacturer. RNA integrity was assessed by agarose-formaldehyde gel electrophoresis. In total, 400 ng of RNA and random decamers (Invitrogen) were used to synthesize first-strand cDNA by Moloney murine leukemia virus reverse transcriptase (Invitrogen). qRT-PCR negative controls were included for all samples. Expression levels of P1, P2, and P3 subunit c isoforms, before and after silencing, were measured by qRT-PCR. Specific primers for P1 (Hs_ATP5G1_1_SG QuantiTect Primer Assay), P2 (Hs_ATP5G2_1_SG QuantiTect Primer Assay), and P3 (Hs_ATP5G3_1_SG QuantiTect Primer Assay) from GeneGlobe (QIAGEN) were used. A standard curve of known amounts of DNA template was generated by PCR to quantify the respective amounts of each isoform. The DNA was gel purified and quantified by spectrometry.

Immunofluorescence Microscopy

Cells were grown on coverslips, fixed in 4% paraformaldehyde, permeabilized with 0.1% Triton-X100, and blocked with 5% bovine serum albumin (BSA). Primary antibodies were added for 1 h at 37°C in phosphate-buffered saline (PBS) containing 10% goat serum, 1% BSA, and 0.1% Triton X-100. After washing, cells were incubated with appropriate cyanine (Cy)2 and Cy3-conjugated secondary antibodies (Jackson ImmunoResearch Laboratories, West Grove, PA), and mounted in immunofluorescence mounting medium (Fluoromount; Southern Biotechnology Associates, Birmingham, AL). Anti-HA and anti-myc antibodies were used (Abcam, Cambridge, MA). Samples were analyzed using an LSM510 laser scanning confocal microscope (Carl Zeiss Microimaging, Thornwood, NY) equipped with a 63×/1.25 numerical aperture oil lens. A series of z-sections were taken spanning the thickness of the cell, with intervals between sections set at 0.7 μm. The z-stack images were projected onto a single plane using the LSM Image Browser software (Carl Zeiss MicroImaging). Digital magnification was 2× (total magnification was 126×). To label mitochondria, 25 nM MitoTracker Red (Invitrogen) was added to the medium for 25 min at 37°C, followed by a quick wash in PBS and fixation. To study mitochondrial morphology and distribution, images from at least 20 random fields from three independent experiments were taken and analyzed.

Biochemical Assays

ATP synthesis was measured in digitonin-permeabilized cells by using a luciferin–luciferase method with malate plus pyruvate as substrates, as described previously (Vives-Bauza *et al.*, 2007). Cytochrome *c* oxidase (COX)-dependent ATP synthesis was measured as described above, but using reduced cytochrome c (Sigma-Fluka, St. Louis, MO) in excess (0.14 mM) to prevent self-oxidation, in the presence of 5 nM rotenone. Oxygen consumption in intact cells was measured with a Clark-type electrode (Hansatech Instruments, King's Lynn, Norfolk, United Kingdom) in an oxygraph chamber, as described previously (D'Aurelio *et al.*, 2001). To inhibit mitochondrial respiration, 1.5 mM KCN was added. *N*,*N*,*N*′,*N*′-Tetramethyl-*p*-phenylendiamine (TMPD)-dependent respiration was measured in whole cells in the presence of 20 nM antimycin A (Sigma-Aldrich) and 2 mM TMPD (Sigma-Fluka). Citrate synthase and COX enzymatic activities were measured spectrophotometrically on cell lysates (50 μg of protein) as described previously (Birch-Machin and Turnbull, 2001).

Preparation of Mitochondria Fractions

Mitochondria were isolated according to procedures described previously (Chomyn, 1996). Cells were incubated for 3 min in 10 mM Tris-HCl, pH 6.7, 10 mM KCl, and 1.5×10^{-4} M $MgCl_2$ and homogenized in a Potter-Elvehjem homogenizer. Sucrose was added to the homogenate to 0.25 M final concentration. The homogenate was then centrifuged for 5 min at $1200 \times g$ to remove large debris and nuclei. Mitochondria were collected by centrifugation for 10 min at $8000 \times g$.

Western Blot Analyses

Fifty micrograms of protein was separated by 12.5% SDS-polyacrylamide gel electrophoresis (PAGE) and electroblotted onto polyvinylidene difluoride (PVDF) filters (Bio-Rad Laboratories, Hercules, CA). Antibodies against different subunits of the oxidative phosphorylation complexes were obtained from Invitrogen. The antibody against subunit a was a kind gift from Dr. Eric Schon (Columbia University, New York, NY).

Blue Native Electrophoresis (BN-PAGE)

Mitochondrial membranes were isolated from 2.5×10^6 cells as described previously (Nijtmans *et al.*, 2002). Cells were solubilized with 3% digitonin (wt/vol) (Sigma-Aldrich) and 0.4% (wt/vol)lauryl maltoside (Sigma-Aldrich). Ten microliters of samples were electrophoresed on a 5–13% gradient polyacrylamide gel as described previously (Nijtmans *et al.*, 2002). Transfer of proteins onto a PVDF membrane (Bio-Rad Laboratories) was carried out overnight at 30 V at 4°C. For second-dimension gel electrophoresis, a lane excised from the first dimension native gel was first treated for 30 min with denaturing buffer containing 15 mM β-mercaptoethanol and 1% SDS and then washed in 1% SDS for 1 h. The gel strip was electrophoresed on a tricine-SDS-polyacrylamide gel as described previously (Brookes *et al.*, 2002). For immunodetection of proteins and protein complexes, monoclonal antibodies against the following subunits were used: 39 kDa of complex I, 70 kDa of complex II, core 2 of complex III, subunit I and subunit IV of complex IV, and β-subunit of complex V (all from Invitrogen). A6 subunit of complex V was detected with a rabbit polyclonal antibody (a gift from Dr. Eric Schon, Columbia University). Quantification of respiratory chain complexes was performed from Western blots by densitometric analyses by using the Scion2 image software (Scion, Frederick, MD).

Live Cell Mitochondrial Transmembrane Potential ($\Delta\Psi_m$) Microscopy and Tetramethyl Rhodamine Methyl Ester Fluorescence Quantification

For live cell imaging, cells were grown on four-well chamber slides (Nalge Nunc International, Rochester, NY). To measure $\Delta\Psi_m$, cells first received medium containing 1 mM pyruvate as sole carbon energy source for 1 h, followed by incubation in 10 nM TMRM (Invitrogen) in the same medium for 20 min. Live imaging was performed as described previously (Vives-Bauza *et al.*, 2008). The uncoupling agent carbonyl cyanide *p*-trifluoromethoxyphenylhydrazone (3 mM) was added to the cells to depolarize mitochondria and measure residual, non–$\Delta\Psi_m$-dependent fluorescence, which was subtracted from the initial fluorescence values. All imaging settings were kept constant among all experiments to allow a direct comparison between control and treated cells. At least 100 cells/sample were analyzed in three independent experiments.

Statistical Analyses

Data are expressed as mean ± SD. Comparisons between groups were made using one-way analysis of variance. Pairwise comparisons were made by post hoc Kolmogorov–Smirnov test. Differences were considered statistically significant at $p < 0.05$. Data analyses were performed using the statistical program StatView (Adept Scientific, Letchworth Garden City, Hertfordshire, United Kingdom).

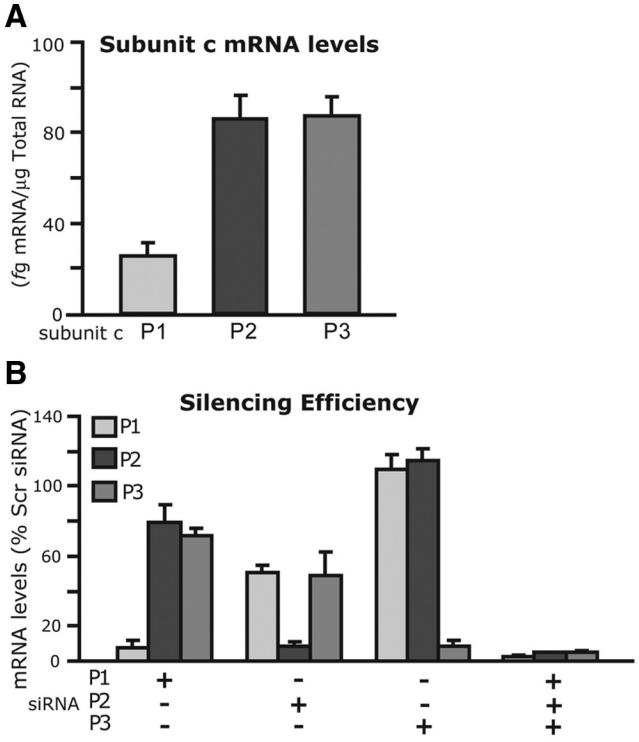

Figure 1. Expression levels of F_1F_0-ATP synthase subunit c isoforms in HeLa cells. (A) Absolute mRNA expression levels of subunit c isoforms in HeLa cells, as measured by quantitative RT-PCR using external standard references; mRNA content is expressed as *f*g of subunit-specific mRNA per μg of total RNA. (B) Quantification of gene silencing efficiency by isoform-specific siRNAs 48 h post-transfection. Values are expressed as a percentage of scrambled control.

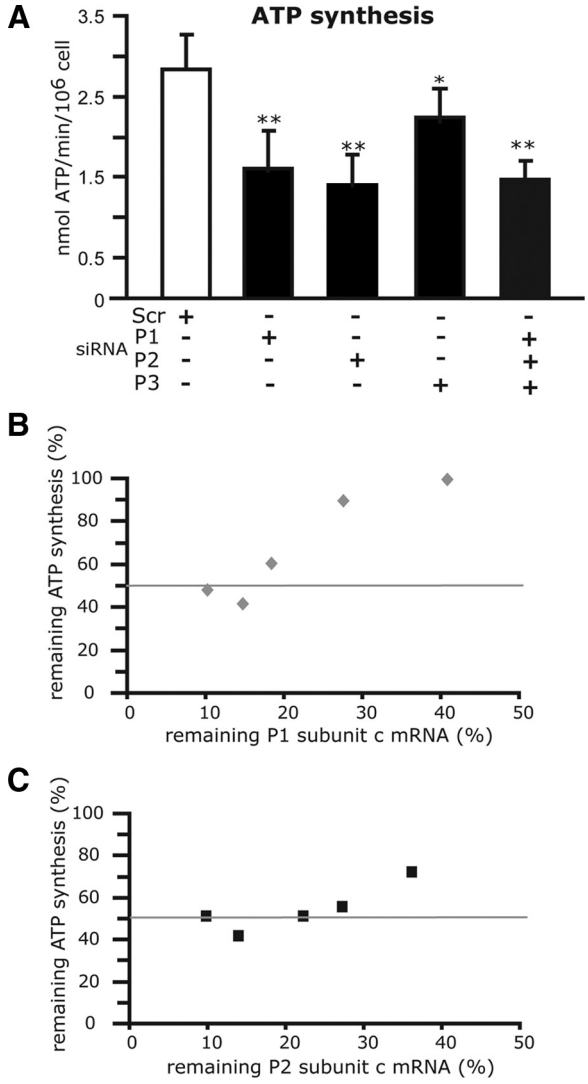

Figure 2. Silencing of individual subunit c isoforms results in ATP synthesis defects. (A) HeLa cells were transfected with specific siRNAs for each subunit c isoform. Mitochondrial ATP synthesis was decreased when any of the isoforms was silenced. Error bars represent ± SD. Five independent experiments were performed. *$p < 0.05$ and **$p < 0.01$ compared with scrambled controls. (B and C) Correlation between residual mRNA levels and ATP synthesis. The line denotes 50% of normal ATP synthesis in HeLa cells transfected with scrambled siRNA. The silencing threshold for causing ATP synthesis defect of 50% or more is higher for P1 (B) than for P2 (C).

RESULTS

Modulation of Subunit c Isoforms Expression in HeLa Cells

We determined the relative expression levels of subunit c isoforms in HeLa cells by qRT-PCR. Amplicons specific for each isoforms were generated with appropriate primer sets and their molecular mass quantified by spectrophotometry. Known amounts of amplicons were used to build qPCR standard curves, which were then used to assess the absolute concentration of each subunit c mRNA. P2 and P3 subunit c were equally expressed and the most abundant, whereas P1 mRNA levels were four times lower (Figure 1A). A similar expression pattern had been shown in mammalian tissues (Gay and Walker, 1985; De Grassi *et al*., 2006).

To investigate their functional requirement, the three isoforms of subunit c were knocked down individually or in combination in HeLa cells, by using siRNA oligonucleotides directed against 5′- or 3′-untranslated regions of the mRNA that are not homologous among the three isoforms. For the P2 isoform, we used a siRNA that targets both variants a and b. Scrambled oligonucleotides were used as controls. Oligonucleotides were delivered by standard lipofection and 48 h after transfection, subunit c isoforms silencing efficiency was estimated by qRT-PCR. The silencing of individual subunit c isoforms resulted in a variable reduction of the corresponding mRNA levels ranging from 80 to 95% of scrambled controls (Figure 1B). The silencing of P1 and P2 was also associated with a moderate (<50%) decrease in the expression of P2 plus P3 and P1 plus P3, respectively. Cross-silencing of the other isoforms was not detected with P3 silencing. Simultaneous silencing resulted in a marked decrease of all three isoforms. Scrambled oligonucleotides had no effect on the expression of subunit c isoforms (data not shown).

Subunit c Isoforms Down-Regulation Causes Oxidative Phosphorylation Impairment

Individual silencing of either P1 or P2 translated into a significant deficit in mitochondrial ATP production (41 ± 18.5%, $p < 0.01$ and 48 ± 11.2%, $p < 0.01$, respectively), measured using malate and pyruvate as substrates, compared with scrambled controls (Figure 2A). Silencing of P3

significantly diminished ATP synthesis by 20 ± 7.4%, $p < 0.05$. When the three isoforms were silenced simultaneously, ATP production was decreased to a similar extent (46 ± 3.7%, $p < 0.01$) than P1 or P2 alone. This result suggests that small residual amounts of subunit c mRNAs are sufficient to maintain approximately half of normal ATP synthesis.

To assess the correlation between subunit c depletion and ATP synthesis defects the silencing efficiency of each isoform was assessed by qRT-PCR concomitantly to every ATP synthesis assay. The correlation plot of residual mRNA levels versus residual ATP synthesis, after P1 or P2 silencing, showed that a silencing efficiency of P1 greater than 80% was necessary to cause an ATP synthesis defect (Figure 2B). Despite the fact that P2 is normally expressed fourfold more than P1, 80% silencing of P1 or P2 translated into similar ATP synthesis defects (Figure 2B). These data indicate that the absolute amounts of P1 and P2 mRNAs needed to maintain 50% ATP synthesis are significantly different.

Recombinant Subunit c Isoforms Can Complement Cognate Isoform Silencing but Cannot Cross-Complement Silencing of Other Isoforms

To exclude that the ATP synthesis defects resulting from subunit c silencing were caused by off-target effects of the siRNAs, we complemented the silenced endogenous isoforms with recombinant subunit c isoforms. P1 and P2 cDNAs were engineered with C-terminal epitope tags P1-HA and P2-myc, respectively (Figure 3A). Recombinant P1 and P2 were not affected by the siRNA oligonucleotides because they lacked the untranslated regions. Both recombinant proteins were correctly targeted to mitochondria, as shown by staining with the mitochondrial specific dye MitoTracker Red and immunocytochemistry in transiently transfected HeLa cells (Figure 3B). Importantly, both P1-HA and P2-myc were assembled in the F_1F_0-ATPase complex, as shown by blue native gel electrophoresis of native mitochondrial protein complexes. The immunoreactive bands detected by the HA or the myc antibodies (Figure 3C) corresponded to the fully assembled F_1F_0-ATPase, detected by antibodies against the β-subunit (Figure 3C). In addition, the antibodies against the tagged recombinant proteins detected a faster migrating band of ~66 kDa, which presumably corresponded to a subunit c subcomplex.

ATP synthesis was assessed in HeLa cells stably expressing P1-HA or P2-myc stably, upon silencing of endogenous P1 or P2, respectively. P1-HA prevented the ATP synthesis impairment induced by endogenous P1 silencing, but failed to restore the effects of P2 silencing (Figure 3D). Similarly, P2-myc prevented the ATP synthesis impairment induced by endogenous P2 silencing but failed to restore the effects of P1 silencing. The lack of cross-complementation between P1 and P2 suggests that these two isoforms are not interchangeable, and thus they are not functionally redundant.

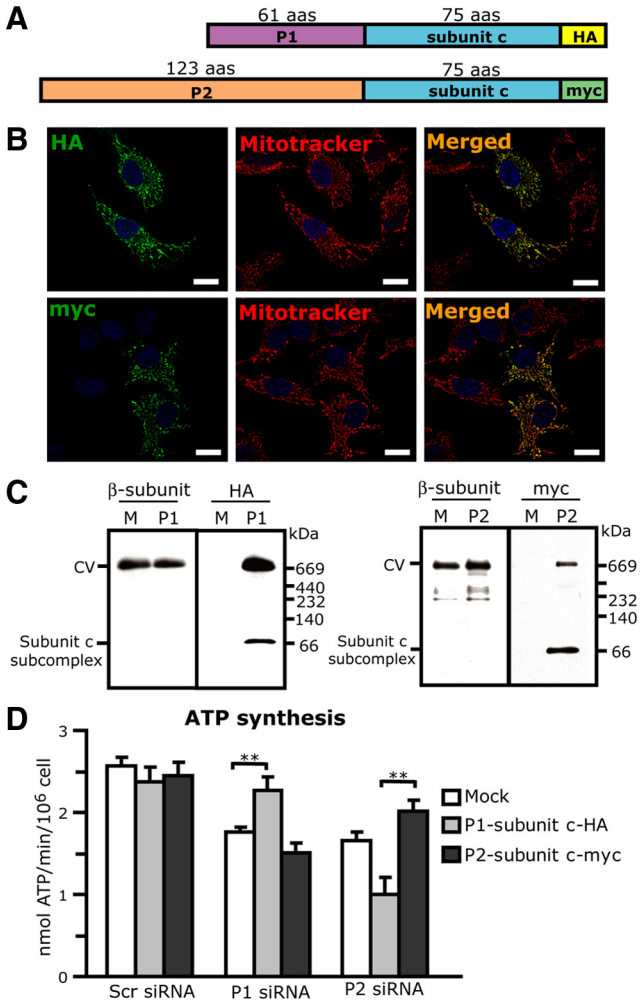

Figure 3. Recombinant subunit c isoforms assemble into complex V and rescue ATP synthesis defects. (A) Schematic diagram of the subunit c constructs used to generate stable HeLa cell lines: P1-subunit c was HA-tagged at the C terminus, whereas P2-subunit c was myc-tagged. (B) P1 and P2-subunit c localized to mitochondria in HeLa cells, as demonstrated by colocalization of HA or myc immunocytochemistry and MitoTracker Red. Bar, 10 μm. (C) P1 and P2-subunit c assembled into complex V (CV), as shown by BN-PAGE. Immunoblotting with β-subunit antibodies identified the fully assembled CV (left side of each panel). Reprobing with anti-Tag antibodies showed assembly of recombinant proteins in the CV, as well as in the subunit c subcomplex. M, mock transfected; P1, P1-subunit c transfected; and P2, P2-subunit c transfected. (D) Measurement of mitochondrial ATP synthesis in HeLa cells after P1 or P2 silencing and expression of recombinant P1 or P2. Recombinant P1-subunit c, but not P2-subunit c, expression rescued the effects of P1-silencing. Similar results were found for P2-subunit c. Error bars represent ± SD. n = 3. **$p < 0.01$ compared with mock-transfected controls.

Subunit c Isoform Silencing Impairs Electron Transport Chain and Alters Mitochondrial Morphology and Distribution

To further explore the functional consequences of silencing P1 and P2, we measured mitochondrial respiration. Interestingly, P2 silencing resulted in a significant deficit of oxygen consumption, which was not observed upon silencing of P1 or P3 (control, 13.2 ± 3.4 vs. P2: 8.1 ± 1.6 μmol O_2/min/10^6 cell, $p < 0.001$) (Figure 4A). The combined silencing of all three subunits also resulted in a respiration defect.

$\Delta\Psi_m$ depends on the coupling between the electron transfer chain activity and the proton translocation in the F_1F_0-ATPase. Thus, as a measure of mitochondrial fitness, we estimated changes in $\Delta\Psi_m$ by using the potentiometric fluorescent dye tetramethyl rhodamine methyl ester (TMRM). We detected a reduction in average TMRM fluorescence upon P1 or P2 silencing (25.2 ± 8%, $p < 0.001$ and 37.5 ± 6.2%, $p < 0.001$, respectively) but not upon P3 silencing (15 ± 16.25%, $p = 0.456$) (Figure 4, B and C), compared with scrambled siRNA controls. Similar results were obtained when all three isoforms were silenced (40 ± 10%, $p < 0.001$).

Because mitochondrial function and metabolic activity influence mitochondrial morphology (Yaffe, 1999; Karbowski and Youle, 2003), we determined the effects of subunit c

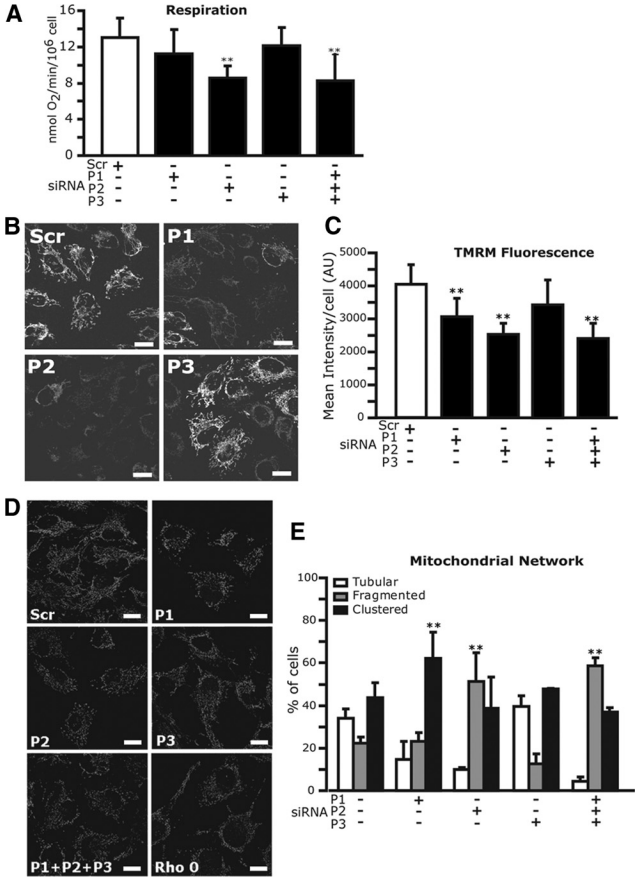

Figure 4. Silencing of subunit c isoforms causes respiratory defects and mitochondrial network alterations. (A) HeLa cells were transfected with the indicated siRNAs and oxygen consumption was measured in intact cells using pyruvate as substrate. Silencing of P2 or all three isoforms (P1, P2, and P3) caused significant respiration defects. (B) Changes in $\Delta\Psi_m$ were assessed by TMRM fluorescence on living cells after silencing of P1, P2, or P3. In the representative examples, note the lower fluorescence in P1 and P2 silenced cells. Scr, scrambled siRNA control. Bars, 10 μm. (C) Quantification of TMRM fluorescence. Silencing of P1 or P2 or all three isoforms (P1, P2, and P3) impaired $\Delta\Psi_m$. (D) Mitochondrial morphology changes after subunit c silencing. The mitochondrial network was labeled with MitoTracker Red. In the representative examples, mitochondria seem mostly clustered or fragmented after silencing P1 or P2. Scr, scrambled siRNA control; Rho0 cells (cell that lack mtDNA) were used as controls. Bars, 10 μm. (E) Analysis of mitochondrial network morphology. Scrambled siRNA-transfected control cells displayed variable mitochondrial network morphology. P1 silencing significantly changed mitochondrial distribution and P2 silencing increased mitochondrial fragmentation. Error bars represent $\pm$ SD. n = 3 independent experiments. In each experiment, at least 50 cells were analyzed. **$p < 0.01$ compared with scrambled controls.

isoforms silencing on the mitochondrial network. We labeled mitochondria with MitoTracker Red and categorized silenced cells based on mitochondrial morphology criteria. Under normal conditions, HeLa cells have variable shape and distribution of the mitochondrial network. Cells normally display a tubular mitochondrial network but can also show clustering of mitochondria around the nucleus or fragmented network with round mitochondria. An excessive clustering or fragmentation is indicative of mitochondrial dysfunction. For comparison, rho0 cells (mitochondrial DNA-less cells), which are devoid of respiratory chain and

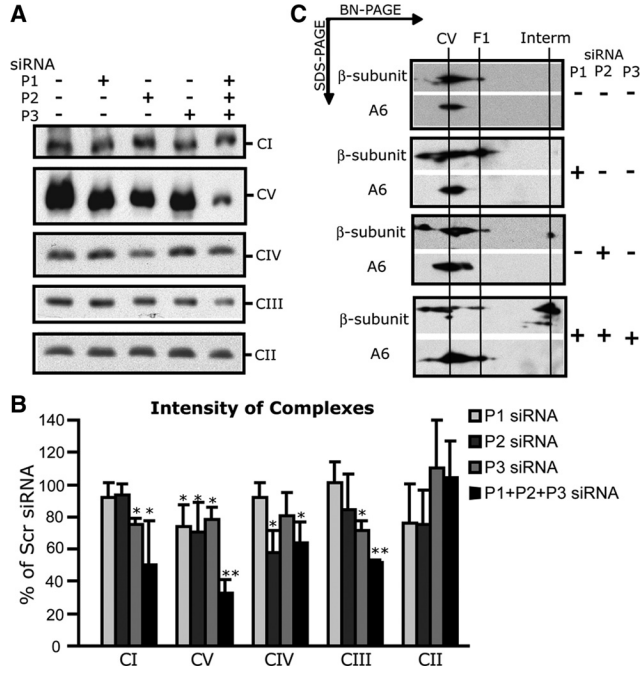

Figure 5. Silencing of subunit c isoforms alters the assembly of the oxidative phosphorylation complexes. (A) BN-PAGE followed by immunoblotting for complexes I-V in HeLa cells. (B) After digital scanning of the immunoblots (n = 4), the band intensities of the different complexes were plotted as a percentage of scrambled siRNA transfected controls. Silencing of individual isoforms resulted in partial disassembly of different respiratory chain complexes. *$p < 0.05$, **$p < 0.01$ compared with scrambled controls. (C) SDS-PAGE second dimension of a BN-PAGE gel immunoblotted with an antibody against the β-subunit of F_1F_0-ATP synthase to identify complex V (CV). Accumulation of assembly intermediates of CV (F1 and Interm) was observed in cells depleted of P1 or P2. The assembly of A6 does not seem to be affected by individual P1 or P2 silencing, whereas assembly intermediates containing A6 occur in the triple-silenced cells.

have low $\Delta\Psi_m$, had a completely fragmented mitochondrial network (Figure 4D). P1 silencing caused a decrease in the number of cells with tubular network and an increase of cells with clustered mitochondria as compared with scrambled control (control, 42 $\pm$ 3% vs. P1 silence, 61 $\pm$ 6%, $p < 0.001$) (Figure 4, D and E). P2 silencing resulted in decreased tubular morphology but also increased fragmentation of the mitochondrial network (control, 21 $\pm$ 2% vs. P2 silence, 52% $\pm$ 10%, $p < 0.001$). The simultaneous silencing of all three subunit c isoforms resulted in an almost complete loss of cells with tubular mitochondria and an increase in cells with fragmented mitochondrial network. The silencing of P3 alone did not affect mitochondrial morphology significantly.

Subunit c Silencing Impairs Oxidative Phosphorylation Complexes Assembly

The differences observed in oxidative phosphorylation function and mitochondrial morphology when silencing individual subunit c isoforms prompted us to investigate the assembly of the oxidative phosphorylation system complexes by BN-PAGE and Western blot. Individual silencing of each of the three subunit c isoforms translated into a similar modest destabilization of ATPase (Figure 5A). Densitometric analyses revealed a reduction in the content of fully assembled ATPase (P1, 17.3 $\pm$ 2.5%, $p < 0.05$; P2, 23.5 $\pm$ 4.7%, $p < 0.05$; and P3, 21.4 $\pm$ 2.1%, $p < 0.05$) (Figure 5B).

However, when all three isoforms were silenced simultaneously, the ATPase was more severely reduced (67.4 ± 9.1%, $p < 0.001$) (Figure 5, A and B). The two-dimension Western blot, where complexes were first separated by BN-PAGE and then by denaturing electrophoresis, demonstrated that silencing of the individual subunits resulted in accumulation of assembly intermediates, as shown by β-subunit immunoreactivity (Figure 5C). Similarly, the triple silencing caused the increase of F1 subcomplexes. Conversely, the assembly of the mitochondrial DNA (mtDNA)-encoded A6 subunit of the F_0 was unaffected by silencing of any subunit c isoform, indicating that A6 is assembled independently of F_1. Clearly, the ATP synthesis defects observed upon silencing of P1 and P2 (Figure 2A) do not directly correlate with the levels of assembled ATPase, because, despite having much less ATPase, the triple-silenced cells had a similar ATP synthesis defect as the individually silenced cells. Moreover, P3 silencing induced the same lack of accumulation of assembled ATPase than P1 or P2 silencing, but it did not translate into a severe ATP synthesis defect (Figure 2, A and 5). Together, these results indicate that the levels of residual ATPase alone cannot explain the differences in ATP synthesis observed among cells subjected to silencing of the various subunit c isoforms. Thus, we investigated the assembly of the respiratory chain complexes. Interestingly, although silencing of P1 did not affect any of the complexes, P3 silencing caused a reduction in complexes I (24.7 ± 1.3%, $p < 0.05$) and III (28.6 ± 2.5%, $p < 0.05$); P2 silencing decreased complex IV by 42 ± 9.6% ($p < 0.01$); and the triple silencing decreased complexes I (49.4 ± 26.8%, $p < 0.05$), III (48.6 ± 1.6%, $p < 0.01$), and IV (36.3 ± 7.5%, $p < 0.01$). Therefore, the subunit c isoforms play a role in the assembly or the stabilization of the respiratory chain complexes.

Silencing of P2-Subunit c Impairs Complex IV

Silencing of P2 caused decreased cell respiration and complex IV disassembly (Figures 4A and 5, A and B). To further investigate the extent of complex IV deficiency, we first silenced P2 and fixed and immunostained cells for COX-I (subunit I of complex IV). A large proportion of cells (40%) had a loss of COX-I immunostaining (Figure 6A). Western blot analyses confirmed a decrease in the steady-state levels of COX-I in P2-silenced cells (Figure 6B). Then, using two-dimension electrophoresis and two different antibodies against complex IV subunits (COX-I and COX-IV), we revealed an increased accumulation of assembly intermediates upon P2 silencing (Figure 6C). Furthermore, TMPD-dependent respiration in the presence of antimycin A, which measures complex IV activity, was significantly decreased in P2 and triple-silenced cells (control, 11.8 ± 0.5 vs. P2: 6.5 ± 1.4; P123, 7.8 ± 1.6 μmol O_2/min/10^6 cell, $p < 0.001$) (Figure 6D). Spectrophotometric measurements, using reduced cytochrome *c* as substrate, confirmed decreased complex IV activity in P2-silenced cells relative to citrate synthase, a Krebs cycle enzyme (Figure 6E). P1-silenced cells did not exhibit a TMPD-dependent respiration defect, indicating that complex IV was functionally intact (Figure 6D). However, when ATP synthesis was measured using reduced cytochrome c in the presence of rotenone, P1 silenced cells were defective compared with scrambled controls (control, 2.5 ± 0.3 vs. P1: 2.0 ± 0.34 nmol ATP/min/10^6 cell, $p < 0.001$) (Supplemental Figure 1), suggesting that loss of P1 affects components of the phosphorylation machinery downstream of complex IV.

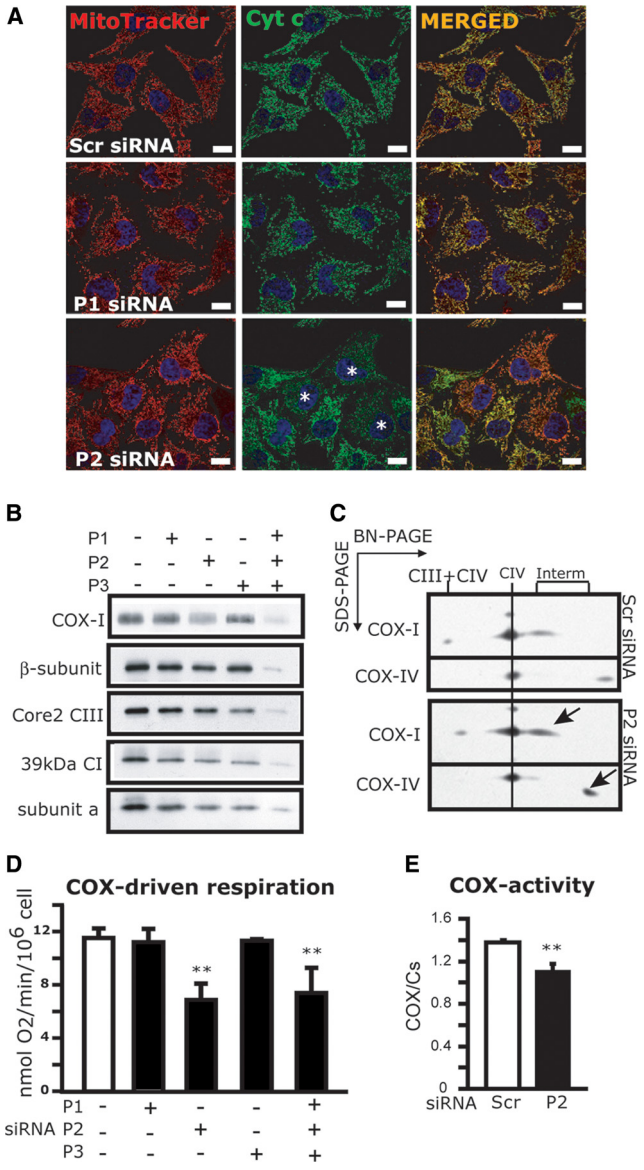

Figure 6. Silencing of P2 induces a complex IV deficiency. (A) HeLa cells were immunostained for COX-I subunit of complex IV (in green) and mitochondria were labeled with MitoTracker Red. Asterisks indicate cells with low COX-I in P2 silenced cells. Bar, 10 μm (B) COX-I subunit of complex IV is down-regulated in P2-silenced cells. Western blot analysis of whole cell lysates from HeLa cells 48 h postsilencing subunit c isoforms. A mixture of antibodies was used: anti-39 kDa subunit for complex I, anti-70 kDa subunit for complex II, anti-core 2 for complex III, anti-CO I for complex IV, anti-β-subunit and anti-subunit a for complex V. (C) SDS-PAGE second-dimension immunoblotted with COX-I and COX-IV antibodies showed accumulation of assembly intermediates of complex IV in P2-silenced cells (arrows). (D) Oxygen consumption was measured in intact cells by using 2 mM TMPD in the presence of 20 nM antimycin A to reveal the specific activity of complex IV. TMPM-dependent respiration was decreased in P2-silenced and triple-silenced cells. n = 3. **$p < 0.01$ compared with scrambled controls. (E) Cytochrome *c* oxidase activity is impaired in P2-silenced cells. Enzymatic cytochrome *c* oxidase activity was measured spectrophotometrically using specific substrates. Citrate synthase (Cs) activity was used to normalize the mitochondrial levels.

Expression of the Respective Targeting Peptides Rescues the Oxidative Phosphorylation Defect Induced by Silencing of P1 or P2

Silencing of P1 and P2 resulted in oxidative phosphorylation deficiency, and recombinant P1 and P2 were unable to cross-complement (Figures 2–4). Because P1 and P2 only differ by their targeting peptides, which drive import of subunit c into mitochondria, these presequences could play a specific role in oxidative phosphorylation function. To explore this hypothesis, we generated fusion proteins containing P1 or P2 targeting peptides in front of EYFP or ECFP, respectively. The fusion proteins were expressed in HeLa cells, where mitochondria contained mostly the processed peptides, as shown by Western blot analyses of subcellular fractions (Supplemental Figure 2). This suggests that P1 or P2 fusion proteins were imported and processed in the mitochondrial matrix. We then transiently transfected HeLa cells in which endogenous P1 or P2 had been silenced with P1 or P2 fusion proteins, and we studied changes in $\Delta\Psi_m$ as a readout of mitochondrial respiratory chain function. The mitochondrially targeted fluorescent proteins did not affect TMRM fluorescence, when expressed in scrambled controls (Figure 7, A and B). When P1-EYFP was expressed in P1-silenced cells, $\Delta\Psi_m$ was restored to normal levels (compare P1-silenced cells transfected with mock, 1543 ± 14 vs. P1-EYFP, 2320 ± 36 arbitrary units (AU), $p < 0.001$) (Figure 7A). Similarly, in P2-silenced cells, P2-ECFP significantly improved $\Delta\Psi_m$ (compare P2-silenced cells transfected with mock, 1503 ± 26 vs. P2-ECFP, 2006 ± 12 AU, $p < 0.001$) (Figure 7B). Interestingly, P1-EYFP or P2-ECFP expression failed to cross-complement the loss of $\Delta\Psi_m$ in P2- or P1-silenced cells, respectively (Figure 7, A and B).

To further investigate the functional complementation effects of the targeting peptides in P1 or P2 silenced cells, we generated HeLa cells stably expressing either P1-A6-FLAG or P2-ECFP. P1-A6-FLAG expression prevented the ATP synthesis deficit caused by P1 (1.6 ± 0.03 vs. 2.3 ± 0.2 nmol ATP/min/10^6 cell, $p < 0.001$) but not by P2 silencing (1.6 ± 0.07 vs. 1.4 ± 0.1 nmol ATP/min/10^6 cell, $p = 0.4$) (Figure 7C). Similarly, in P2-ECFP–expressing cells, P2 silencing-induced ATP synthesis defect was prevented (1.0 ± 0.014 vs. 2.1 ± 0.11 nmol ATP/min/10^6 cell, $p < 0.001$) (Figure 7D).

Together, these results indicate that the targeting signals are sufficient to rescue the oxidative phosphorylation defects induced by silencing of the respective subunit c isoforms and suggest novel functional roles for P1 and P2 targeting peptides in oxidative phosphorylation.

P2 Targeting Peptide Restores Complex IV Assembly and Function in P2-silenced Cells

Because we identified a complex IV assembly defect in P2-silenced cells associated with decreased mitochondrial respiration (Figures 4–6), we tested whether exogenous P2 expression could rescue these defects. COX-dependent respiration was significantly ameliorated in P2 silenced cells stably expressing P2-ECFP (compare P2-silenced cells transfected with mock, 16.1 ± 1.0 vs. P2-ECFP, 22.2 ± 1.6 μmol O_2/min/10^6 cell, $p < 0.001$) (Figure 8A). BN-PAGE demonstrated that complex IV assembly was normalized in P2-silenced cells stably expressing P2-ECFP (Figure 8B). The second dimension of the BN-PAGE showed that P2-ECFP expression prevented the accumulation of complex IV assembly intermediates, upon P2 silencing (compare P2 silenced cells transfected with mock, 105.7 ± 73.2 vs. P2-ECFP, 352.9 ± 133.3 AU, $p < 0.001$) (Figure 8, C and D). Therefore, P2 targeting peptide plays a critical role in the assembly of complex IV in mammalian cells.

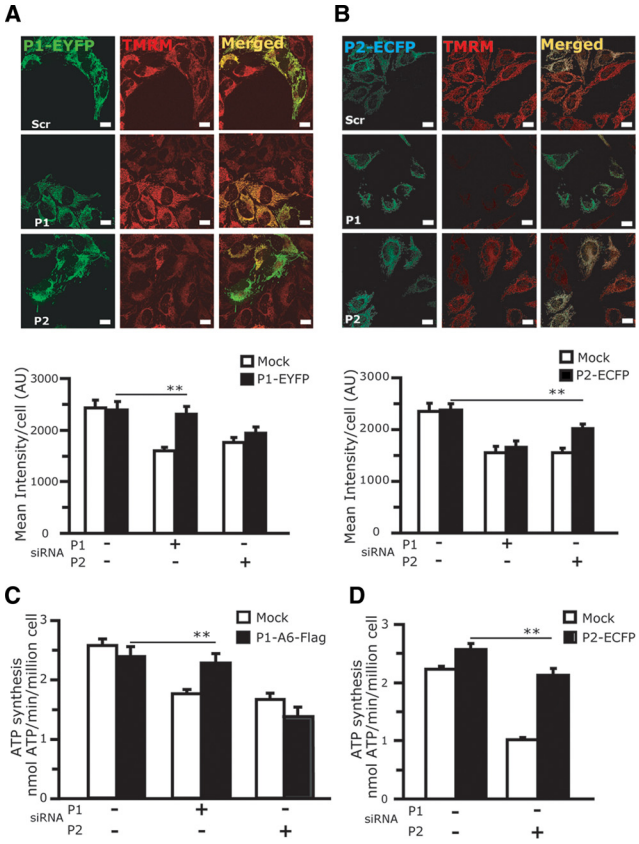

Figure 7. P1 or P2 targeting peptides rescue the mitochondrial dysfunction caused by silencing of the respective subunit c isoforms. Representative changes in $\Delta\Psi_m$ assessed by TMRM staining in cells transfected with P1-EYFP (A) or P2-ECFP (B) after silencing of subunit c isoforms. Quantification of TMRM fluorescence is shown below each panel. TMRM fluorescence increased in cells expressing P1-EYFP, when P1 was silenced, and in cells expressing P2-ECFP, when P2 was silenced. n = 3 independent experiments, in each experiment, at least 50 transfected cells were analyzed in each group. **$p < 0.01$, compared with mock transfected controls. Bars, 10 μm. (C and D) Stable cell lines expressing P1-A6-FLAG or P2-ECFP were transfected with scrambled, P1, or P2 siRNAs. ATP synthesis was measured 48 h later using malate plus pyruvate as substrates. ATP synthesis defects induced by P1 or P2 silencing were ameliorated by P1-A6-FLAG and P2-ECFP, respectively. Error bars represent ± SD. n = 3. **$p < 0.01$ with compared with mock-transfected controls.

Based on its known crystal structure, complex IV does not include the P2 targeting peptide. However, to firmly establish that P2 targeting peptide is not an integral component of complex IV, we tested its direct association with complex IV by BN-PAGE. First, to overcome the lack of specific antibodies against P2, we tagged P2 targeting peptide with a HA-tag on its C terminus and removed the last three amino acids of P2 targeting peptide, thereby preventing the cleavage of the HA-Tag (Supplemental Figure 3A). Colocalization of HA-antibody immunofluorescence and MitoTracker labeling in P2-HA transiently transfected cells indicated that P2-HA was stable (i.e., not degraded) and correctly targeted to mitochondria. With BN-PAGE electrophoresis, we did not detect P2-HA comigrating with complex IV (Supplemental Figure 3B) or in association with any other high-molecular-weight complexes. The absence of P2 targeting peptide in the assembled complex IV suggests that P2 targeting signal

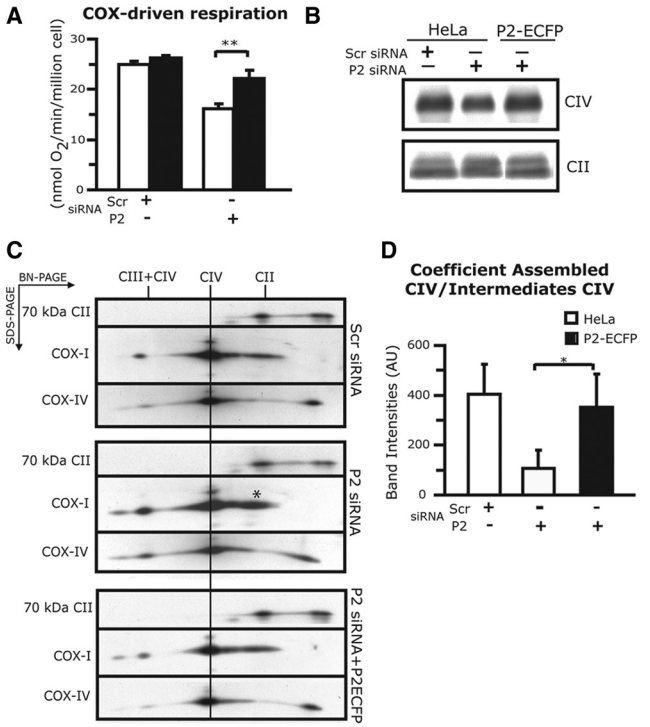

Figure 8. Expression of P2 targeting peptide restores complex IV assembly. (A) HeLa cells stably expressing P2-ECFP or mock controls were transfected with P2 or scrambled siRNA. Oxygen consumption was measured in intact cells using 2 mM TMPD in the presence of 20 nM antimycin A. P2-ECFP improved the TMPD-dependent respiration defect caused by P2 silencing. n = 3. **$p < 0.01$ (B) BN-PAGE immunoblotted with COX-I antibodies. Expression of P2 targeting peptide rescued complex IV (CIV) assembly in P2 silenced cells. Complex II 70-kDa subunit was used as a loading control. (C) SDS-PAGE second-dimension of a BN-PAGE immunoblotted with antibodies against CIV (COX-I and COX-IV). The accumulation of CIV assembly intermediates (asterisk) induced by P2 silencing is ameliorated by the expression of P2-ECFP. Complex II 70-kDa subunit was used as a loading control. (D) Densitometric quantification of ratio between the fully assembled CIV and its assembly intermediates. n = 3, *$p < 0.05$.

may work as a soluble assembly factor rather than a structural subunit of the complex.

DISCUSSION

The evidence presented here support a novel role for the targeting peptides of subunit c of ATPase in mammalian cells. We propose that these peptides serve a dual function. Besides directing subunit c to the correct mitochondrial compartment, the targeting peptides are also involved in regulating the assembly and function of oxidative phosphorylation complexes. Each of the three different targeting peptides for P1, P2, and P3, is likely to serve a unique function, which is consistent with the high amino acid sequence divergence among them. Therefore, our findings provide a mechanistic explanation for the apparent genetic redundancy of the subunit c isoforms.

Our conclusions are supported by three main lines of evidence. First, silencing of each individual subunit c isoform translates into oxidative phosphorylation dysfunction, despite high expression of the remaining subunits, suggesting that the isoforms are not functionally interchangeable. Second, silencing of individual subunit c isoforms results in oxidative phosphorylation defects that involve not just the ATPase, but also other complexes, particularly complex IV in the case of P2. Third, expression of chimeric constructs made of P1 and P2 targeting peptides appended to unrelated proteins, such as ECFP and EYFP, was sufficient to restore oxidative phosphorylation function in cells subjected to subunit c isoform silencing.

There is only one known example of a targeting peptide that plays a direct role in oxidative phosphorylation, the precursor of the Rieske iron–sulfur protein of complex III. This peptide is targeted and assembled into the bovine cytochrome bc_1 complex before being cleaved off, and after cleavage it becomes an integral subunit of the complex as an individual subunit (Brandt *et al.*, 1993; Phillips *et al.*, 1993). Our data do not support the possibility that P2 targeting peptide is a structural component of the complex. Although we cannot completely discard a structural role, we favor the hypothesis that P2 targeting peptide functions as an assembly factor for complex IV. For example, the P2 targeting peptide could provide a protein chaperone activity. P2 accumulated in the matrix could serve to coordinate the insertion of mtDNA-encoded subunits of COX into the mitochondrial membrane together with the nuclear encoded ones. Along this line, a chaperone activity has been described for the targeting peptide of the yeast F_1-ATPase β-subunit (Hajek *et al.*, 1997).

P1 targeting peptide function remains to be identified. In our cellular system, the lack of P1 translated in ATP synthesis and $\Delta\Psi_m$ impairments, which were complemented by the expression of the P1 targeting peptide. We have excluded the Krebs cycle and the respiratory complexes I through IV as potential targets for its role in oxidative phosphorylation maintenance. Respiration driven by TMPD, which in the presence of antimycin A provides electrons directly to cytochrome *c*, was normal in P1 silenced cells. However, COX-driven ATP synthesis measured using reduced cytochrome *c* as substrate was impaired. This suggests a defect of an oxidative phosphorylation component downstream of complex IV. Potential candidates are the ATPase, the adenine nucleotide translocator, or the phosphate carrier. Future studies will be necessary to further understand the involvement of P1 targeting peptide in oxidative phosphorylation.

P3 silencing translated in a milder biochemical phenotype than P1 and P2 silencing. However, it is worth emphasizing that the P3 isoform may be important in maintaining the pool of mature subunit c, because it was the only isoform to be up-regulated upon silencing of the other two isoforms. Therefore, it could be speculated that in HeLa cells P3 targeting peptide may not have major functions besides mitochondrial import. However, unlike the other two isoforms, P3 seems to respond transcriptionally to energy dysfunction.

Paralogue genes are viewed as a source of material for introducing functional novelties into the genome (Yang *et al.*, 2003; Hancock, 2005), and at a present three alternative outcomes are suggested for their evolution: nonfunctionalization (one copy loses its function, being retained just as DNA sequence); neofunctionalization (one copy assumes a completely novel function and is maintained by natural selection); and subfunctionalization (each copy retains some aspect of the original function, and acquires a new function; Lynch and Conery, 2000). Our studies identify, for the first time, ATPase subunit c isoforms as paralogue genes that have evolved by subfunctionalization, adopting new functions through their targeting peptides.

ACKNOWLEDGMENTS

We thank Dr. Eric Schon for the rabbit polyclonal antibody against the subunit a of complex V and Dr. Mrudula Donepudi for the ECFP and EYFP plasmids. This work was supported by National Institutes of Health/National Institute of Neurological Disorders and Stroke and Muscular Dystrophy Association (G. M.), by the Spanish "Fondo de Investigacion Sanitaria" FIS PI07/0347 (to A.L.A. and C.V.B.), and by a fellowship of the Ministerio de Educación y Ciencia Fulbright program from the Spanish Ministry of Education and Science and CIBERER (to C.V.B.).

REFERENCES

Altendorf, K., Stalz, W., Greie, J., and Deckers-Hebestreit, G. (2000). Structure and function of the F(0) complex of the ATP synthase from *Escherichia coli*. J. Exp. Biol. *203*, 19–28.

Birch-Machin, M. A., and Turnbull, D. M. (2001). Assaying mitochondrial respiratory complex activity in mitochondria isolated from human cells and tissues. Methods Cell Biol. *65*, 97–117.

Boyer, P. D. (2000). Catalytic site forms and controls in ATP synthase catalysis. Biochim. Biophys. Acta *1458*, 252–262.

Brandt, U., Yu, L., Yu, C. A., and Trumpower, B. L. (1993). The mitochondrial targeting presequence of the Rieske iron-sulfur protein is processed in a single step after insertion into the cytochrome bc1 complex in mammals and retained as a subunit in the complex. J. Biol. Chem. *268*, 8387–8390.

Brookes, P. S., Pinner, A., Ramachandran, A., Coward, L., Barnes, S., Kim, H., and Darley-Usmar, V. M. (2002). High throughput two-dimensional blue-native electrophoresis: a tool for functional proteomics of mitochondria and signaling complexes. Proteomics *2*, 969–977.

Bulygin, V. V., Duncan, T. M., and Cross, R. L. (2004). Rotor/Stator interactions of the epsilon subunit in *Escherichia coli* ATP synthase and implications for enzyme regulation. J. Biol. Chem. *279*, 35616–35621.

Chomyn, A. (1996). In vivo labeling and analysis of human mitochondrial translation products. Methods Enzymol. *264*, 197–211.

D'Aurelio, M., Pallotti, F., Barrientos, A., Gajewski, C. D., Kwong, J. Q., Bruno, C., Beal, M. F., and Manfredi, G. (2001). In vivo regulation of oxidative phosphorylation in cells harboring a stop-codon mutation in mitochondrial DNA-encoded cytochrome c oxidase subunit I. J. Biol. Chem. *276*, 46925–46932.

De Grassi, A., Lanave, C., and Saccone, C. (2006). Evolution of ATP synthase subunit c and cytochrome c gene families in selected metazoan classes. Gene *371*, 224–233.

Dickson, V. K., Silvester, J. A., Fearnley, I. M., Leslie, A. G., and Walker, J. E. (2006). On the structure of the stator of the mitochondrial ATP synthase. EMBO J. *25*, 2911–2918.

Dyer, M. R., Gay, N. J., and Walker, J. E. (1989). DNA sequences of a bovine gene and of two related pseudogenes for the proteolipid subunit of mitochondrial ATP synthase. Biochem. J. *260*, 249–258.

Dyer, M. R., and Walker, J. E. (1993). Sequences of members of the human gene family for the c subunit of mitochondrial ATP synthase. Biochem. J. *293*, 51–64.

Gay, N. J., and Walker, J. E. (1985). Two genes encoding the bovine mitochondrial ATP synthase proteolipid specify precursors with different import sequences and are expressed in a tissue-specific manner. EMBO J. *4*, 3519–3524.

Hajek, P., Koh, J. Y., Jones, L., and Bedwell, D. M. (1997). The amino terminus of the F1-ATPase beta-subunit precursor functions as an intramolecular chaperone to facilitate mitochondrial protein import. Mol. Cell. Biol. *17*, 7169–7177.

Hancock, J. M. (2005). Gene factories, microfunctionalization and the evolution of gene families. Trends Genet *21*, 591–595.

Karbowski, M., and Youle, R. J. (2003). Dynamics of mitochondrial morphology in healthy cells and during apoptosis. Cell Death Differ. *10*, 870–880.

Lynch, M., and Conery, J. S. (2000). The evolutionary fate and consequences of duplicate genes. Science *290*, 1151–1155.

Manfredi, G., Fu, J., Ojaimi, J., Sadlock, J. E., Kwong, J. Q., Guy, J., and Schon, E. A. (2002). Rescue of a deficiency in ATP synthesis by transfer of MTATP6, a mitochondrial DNA-encoded gene, to the nucleus. Nat. Genet. *30*, 394–399.

Nijtmans, L. G., Henderson, N. S., and Holt, I. J. (2002). Blue Native electrophoresis to study mitochondrial and other protein complexes. Methods *26*, 327–334.

Phillips, J. D., Graham, L. A., and Trumpower, B. L. (1993). Subunit 9 of the *Saccharomyces cerevisiae* cytochrome bc1 complex is required for insertion of EPR-detectable iron-sulfur cluster into the Rieske iron-sulfur protein. J. Biol. Chem. *268*, 11727–11736.

Saccone, C., Lanave, C., and De Grassi, A. (2006). Metazoan OXPHOS gene families: evolutionary forces at the level of mitochondrial and nuclear genomes. Biochim. Biophys. Acta *1757*, 1171–1178.

Sangawa, H., Himeda, T., Shibata, H., and Higuti, T. (1997). Gene expression of subunit c(P1), subunit c(P2), and oligomycin sensitivity-conferring protein may play a key role in biogenesis of H+-ATP synthase in various rat tissues. J. Biol. Chem. *272*, 6034–6037.

Vives-Bauza, C., Anand, M., Shirazi, A. K., Magrane, J., Gao, J., Vollmer-Snarr, H. R., Manfredi, G., and Finnemann, S. C. (2008). The age lipid A2E and mitochondrial dysfunction synergistically impair phagocytosis by retinal pigment epithelial cells. J. Biol. Chem. *283*, 24770–24780.

Vives-Bauza, C., Yang, L., and Manfredi, G. (2007). Assay of mitochondrial ATP synthesis in animal cells and tissues. Methods Cell Biol. *80*, 155–171.

Walker, J. E., and Dickson, V. K. (2006). The peripheral stalk of the mitochondrial ATP synthase. Biochim. Biophys. Acta *1757*, 286–296.

Wittig, I., and Schagger, H. (2008). Structural organization of mitochondrial ATP synthase. Biochim. Biophys. Acta *1777*, 592–598.

Yaffe, M. P. (1999). The machinery of mitochondrial inheritance and behavior. Science *283*, 1493–1497.

Yan, W. L., Lerner, T. J., Haines, J. L., and Gusella, J. F. (1994). Sequence analysis and mapping of a novel human mitochondrial ATP synthase subunit 9 cDNA (ATP5G3). Genomics *24*, 375–377.

Yang, J., Lusk, R., and Li, W. H. (2003). Organismal complexity, protein complexity, and gene duplicability. Proc. Natl. Acad. Sci. USA *100*, 15661–15665.